Review of Die-Attach Materials for SiC High-Temperature Packaging

Hou, Fengze; Sun, Zhanxing; Su, Meiying; Fan, Jiajie; You, Xiangan; Li, Jun; Wang, Qidong; Cao, Liqiang; Zhang, Guoqi

DOI
10.1109/TPEL.2024.3417529

Publication date
2024

Document Version
Final published version

Published in
IEEE Transactions on Power Electronics

Citation (APA)
Hou, F., Sun, Z., Su, M., Fan, J., You, X., Li, J., Wang, Q., Cao, L., & Zhang, G. (2024). Review of Die-Attach Materials for SiC High-Temperature Packaging. *IEEE Transactions on Power Electronics*, *39*(10), 13471-13486. https://doi.org/10.1109/TPEL.2024.3417529

Review of Die-Attach Materials for SiC High-Temperature Packaging

Fengze Hou, *Senior Member, IEEE*, Zhanxing Sun, Meiying Su, Jiajie Fan, *Senior Member, IEEE*, Xiangan You, Jun Li, Qidong Wang, Liqiang Cao, *Senior Member, IEEE*, and Guoqi Zhang, *Fellow, IEEE*

***Abstract*—Silicon carbide (SiC) devices have shown definite advantages over Si counterparts in high-temperature, high-voltage, and high-frequency applications. To fully exploit the potentiality of SiC devices in high temperatures, die-attach materials that can withstand high temperatures for a long time are required in the power electronics packaging. In this article, the high-temperature die-attach materials, such as high-temperature solders and transient liquid-phase bonding materials, were reviewed first. Then, metallic (mainly Ag and Cu) nanoparticles (NPs) sintering technologies were thoroughly overviewed. The metallic NPs sintering materials, metallic NPs sintering process, and interface and reliability were analyzed, respectively. Finally, the challenges and outlook of promising Cu NPs sintering technology were discussed.**

***Index Terms*—Cu nanoparticles (NPs) sintering, die-attach, high-temperature, power electronics packaging, silicon carbide (SiC) devices.**

I. Introduction

As a potential wideband gap semiconductor material, silicon carbide (SiC) offers several superior performances, e.g., wider bandgap, higher breakdown field, thinner drift-layer thickness, lower on-resistance, higher thermal conductivity, and higher switching speed [1], [2]. Owing to a wider bandgap, higher melting point, and thermal conductivity of 4H-SiC material compared with Si, SiC devices can operate at higher temperatures (> 300 °C). Therefore, SiC devices have shown definite advantages in high-temperature applications over Si counterparts.

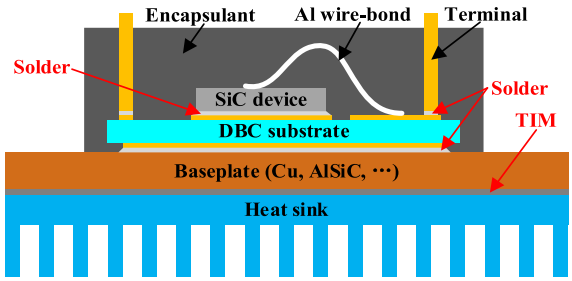

Fig. 1. Schematic of the conventional wire-bonded packaging technology for SiC power devices.

Fig. 1 shows the schematic diagram of current mainstream packaging technology for SiC power devices. As shown in the figure, the bottom side of an SiC device is soldered to a direct-bonded copper (DBC) ceramic substrate. Afterward, the top pad of the SiC device is wire bonded to the DBC substrate to establish the electrical connection between the device and the DBC substrate. The DBC substrate is then soldered to a baseplate, and load terminals and control connectors are soldered to the DBC substrate. The entire assembly is finally enclosed in an encapsulant to protect the internal structures of the SiC power module [3]. For heat dissipation, the SiC wire-bonded package is assembled to a heat sink through a layer of thermal interface material. During the bonding process, the melting-point temperature of the solder should be lower than the previous one.

The conventional die-attach solder materials, such as tin–silver–copper, cannot be used at temperatures over 200 °C and are not suitable for SiC high-temperature packaging. High-lead solder, which contains over 85% lead, is currently excluded from the restriction of hazardous substances directive [4].

To fully exploit the potentiality of SiC devices in high temperatures, die-attach materials that can withstand high temperatures for a long time are required. Currently, the high-temperature die-attach materials mainly include high-temperature solders, transient liquid-phase (TLP) bonding materials, and Ag and Cu nanoparticles (NPs) sintering materials [5], [6], [7].

In recent years, there have been some reviews on high-temperature die-attach materials. Zhang et al. [7] reviewed the pros and cons of high-temperature lead-free solders and sintered Ag. Manikam and Cheong [8] overviewed the high-temperature

Manuscript received 22 April 2024; revised 16 May 2024; accepted 14 June 2024. Date of publication 21 June 2024; date of current version 4 September 2024. This work was supported by the National Natural Science Foundation of China under Grant 62174177. Recommended for publication by Associate Editor K. Ngo. *(Fengze Hou and Zhanxing Sun contributed equally to this work.) (Corresponding authors: Fengze Hou; Qidong Wang; Liqiang Cao.)*

Fengze Hou, Meiying Su, Xiangan You, Jun Li, Qidong Wang, and Liqiang Cao are with the Institute of Microelectronics of the Chinese Academy of Sciences, Beijing 100029, China (e-mail: houfengze@ime.ac.cn; sumeiying@ime.ac.cn; youxiangan@ime.ac.cn; lijun@ime.ac.cn; wangqidong@ime.ac.cn; caoliqiang@ime.ac.cn).

Zhanxing Sun is with the Institute of Microelectronics of the Chinese Academy of Sciences, Beijing 100029, China, and also with the School of Integrated Circuits, University of Chinese Academy of Sciences, Beijing 101408, China (e-mail: sunzhanxing@ime.ac.cn).

Jiajie Fan is with the Institute of Future Lighting, Academy for Engineering and Technology, Fudan University, Shanghai 200433, China, also with the Shanghai Engineering Technology Research Center of SiC Power Device, Fudan University, Shanghai 200433, China, and also with the Research Institute of Fudan University in Ningbo, Ningbo 315336, China (e-mail: jiajie_fan@fudan.edu.cn).

Guoqi Zhang is with the Department of Microelectronics Engineering, Delft University of Technology, 2628 Delft, The Netherlands (e-mail: g.q.zhang@tudelft.nl).

Color versions of one or more figures in this article are available at https://doi.org/10.1109/TPEL.2024.3417529.

Digital Object Identifier 10.1109/TPEL.2024.3417529

TABLE I
MATERIAL PROPERTIES OF HIGH-TEMPERATURE SOLDERS

Materials	Melting point (°C)	Processing temp. (°C)	Thermal conductivity (W/m·K)	CTE (ppm/°C)
Sn5Sb [11]	235	275	28	27
Bi-Ag	262	300	9	20
Au80Sn20 [12]	280	320	57	16
Au88Ge12 [12]	356	386	44	12
Au97Si3 [12]	363	380–400	27	12
Zn-12Al	381	420	110	24
Zn-Al-Mg [14]	350	390	43	24
Zn-Al-Ge [14]	362	400	60	20
Zn-Al-Ge-Mg [14]	375	415	66	25

die-attach materials in high-temperature applications. Siow [9] introduced key thermodynamic and kinetic concepts of TLP, discussed potential applications, and compared them with other die-attach technologies. Chen and Siow [10] compared the mechanical strength and reliability of sintered Ag and Cu and studied the effect of the sintering process on bonding strength. However, there are few reviews of die-attach materials for SiC high-temperature packaging.

The rest of this article is organized as follows. In Section II, high-temperature solders and TLP bonding materials were reviewed. In Section III, metallic (mainly Ag and Cu) NPs sintering technologies were thoroughly surveyed. Metallic NPs sintering materials, metallic NPs sintering process, and interface and reliability were overviewed. In Section IV, the challenges and outlook of Cu NPs sintering technologies were discussed. The challenges of Cu NPs sintering technologies mainly include Cu oxidation issues in the sintering process, tradeoffs among thermal, electrical, and mechanical properties, and inherent effects of pressure, temperature, and time. Finally, Section V concludes this article.

II. HIGH-TEMPERATURE SOLDERS AND TLP BONDING MATERIALS

A. High-Temperature Solders

The high-temperature solders have higher melting points. The processing temperatures are much higher, generally 40 °C higher than the melting points of solders. Table I lists the material properties of several high-temperature solders. Gold-based eutectic die-attach materials, such as Au80Sn20 and Au88Ge12, have been widely used as high-temperature die-attach materials. They melt at 280 °C and 356 °C, respectively. Compared with Au88Ge12, Au80Sn20 possesses better thermal and electrical properties, and hence, it is more commonly used [12]. Although Zn-based solders have higher thermal conductivity, the higher processing temperature presents greater challenges to the manufacturing process [14].

The high-temperature solders seem to be good candidates for SiC high-temperature packaging. However, the reflow cooling down process induces large residue stress and strain and leads to die cracks. Besides, the cost of high-temperature solders is relatively high.

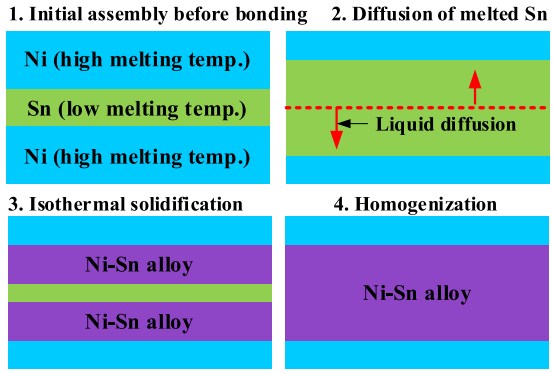

Fig. 2. Schematic diagram of Ni-Sn TLP bonding process [17].

B. TLP Bonding Materials

TLP bonding is a process for the joining of metallic and ceramic materials using an interlayer [15]. It involves the application of a low-melting-point interlayer material, such as Sn or In, between the surface-metalized die and the substrate. As the temperature increases, the interlayer material melts and moves into the lattices and grain boundaries of the die and substrate metallization, forming intermetallic compositions (IMCs). After an annealing process, a homogenized intermetallic bond line can be formed. The intermetallic bond line has a much higher remelt point than the initial interlayer [16]. Fig. 2 illustrates the schematic diagram of a specific Ni-Sn TLP bonding process. The Sn foils are inserted between the power devices and the substrate having pre-existing nickel (Ni) layers. The Sn thickness range is 3–10 μm. The melted Sn diffuses into and reacts with the Ni layers through the solidification process. The process continues until all melted Sn are consumed and transformed to the Ni-Sn alloy having a melting temperature (theoretically ~794 °C) higher than Sn melting temperature (~231 °C) and the maximum process temperature [17].

The TLP bonding combines the features of the conventional soldering and diffusion bonding process [18], [19], [20]. It is a promising die-attach approach for SiC high-temperature packaging because of the following benefits.

1) It can offer excellent joint-filling capability and form a high-quality bond.
2) It can form bonds at a low temperature, thereby minimizing the stress due to the coefficient of thermal expansion (CTE) mismatch between the die and the substrate.
3) It needs relatively low processing pressure (<0.3 MPa) [17], [18], [19], [20], [21].

Many material pairs have been examined for TLP bonding so far. Table II compares different TLP bonding technologies. From the table, the TLP bonding can form different IMCs. Most of them can withstand higher temperatures over 400 °C. However, the pressure and thickness need to be strictly controlled in the TLP bonding process, and longer bonding time is needed

TABLE II
COMPARISON OF TLP BONDING TECHNOLOGIES

Materials	Bonding temp. (°C)	Re-melt temp. (°C)	IMCs	Thermal conductivity (W/m·K)
Au-In [18], [20]	180	AuIn: 509.6; $AuIn_2$: 540.7	AuIn and $AuIn_2$	/
Au-Sn [12]	232	Au_5Sn: 519; AuSn: 419.3	Au_5Sn and AuSn	/
Ag–In [16], [23]	200 180	$AgIn_2$: 400; Ag_2In: 660	$AgIn_2$ Ag_2In	/
Ni-Sn [17], [18], [19], [20], [21], [22], [23], [24], [25]	231	Ni_3Sn_4: 794; Ni_3Sn_2: 1280.	Ni_3Sn_4 and Ni_3Sn_2	/
Cu-Sn [12], [26]	270	Cu_6Sn_5: 415; Cu_3Sn: 676.	Cu_3Sn and Cu_6Sn_5	34–70
Cu @ Sn particle [27]	250	Cu_6Sn_5: 415; Cu_3Sn: 676.	Cu_3Sn and Cu_6Sn_5	127.99–154.26
Cu-Solder-Resin [28]	250	Cu_6Sn_5: 415; Cu_3Sn: 676.	Cu_3Sn and Cu_6Sn_5	23
Sn-In solder ACFs and Au pads [29]	130	380	Au-In-Sn	/
Bi-Ni [30]	271	>400	Bi_3Ni or Bi-Ni intermetallic layer	/
Ag-Sn [12], [31]	300	480	Ag_3Sn	46–60

if we expect higher operating temperatures because forming high-melting-point IMC needs longer reacting time. Generally, low thermal conductivity and high residual stress during bonding are the main issues that need to be improved [9], [22].

III. METALLIC NPS SINTERING TECHNOLOGIES

As the SiC die size tends to be smaller in comparison with the Si counterparts, its heat flux can reach up to 1 kW/cm^2. Such high heat flux cannot be quickly dissipated via high-temperature solders and TLP materials, whose thermal conductivities are generally lower [32], [33]. Ag's extreme thermal conductivity at 0 °C is 428 W/m·K, and Cu comes second at 401 W/m·K. The sintered Ag and Cu have shown higher thermal conductivities compared with other types of die-attach materials, which can reach over 150 W/m·K. Therefore, sintering materials can effectively leverage the performance of SiC devices [8].

When materials are reduced down to the nanoscale, several material characteristics, e.g., melting point [34], surface energy [35], and diffusion coefficient [36], exhibit significant changes compared with their bulk counterparts. Metallic NPs paste sintering has shown fantastic potential in power electronics, especially for die attach due to the following advantages:

1) low-temperature process and high-temperature operation;
2) without liquid phase during sintering and, thus, die shift issues can be avoided;
3) environmentally friendly;
4) excellent thermal, electrical, and mechanical properties [37], [38], [39], [40], [41].

The die shear strength of power modules by sintering NPs paste can achieve above 40 MPa.

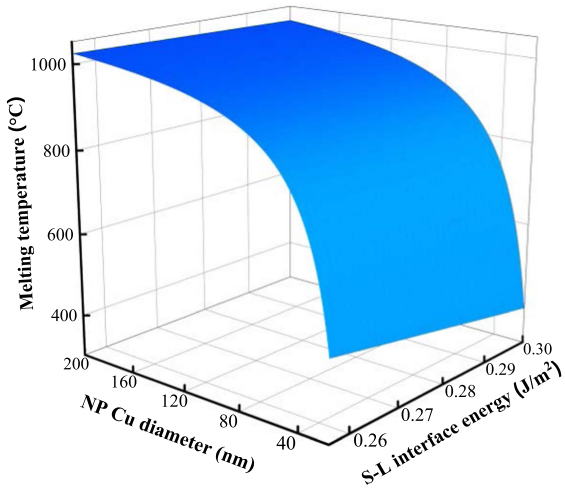

Fig. 3. Melting temperature of NPs Cu dependent on NPs diameter and S-L interface energy.

Metallic NPs paste sintering, fundamentally different from solder alloy reflowing that has solid-to-liquid-phase transition, is defined as the atomic diffusion and NPs consolidation that can happen far below the melting temperatures (T_m) of materials, typically 0.2–0.4T_m [42]. With low sintering temperature, conventional microparticle paste cannot form the dense structure and achieve the desired properties. To improve the density, a high temperature, usually over 750 °C, must be applied to the micron-sized metallic paste [41]. Compared with the conventional microparticles, NPs have higher surface energy and smaller size, which lead to a higher driving force σ for the sintering process as shown in the following equation [43], [44], [45]:

$$\sigma = \gamma\kappa = \gamma\left(\frac{1}{R_1} + \frac{1}{R_2}\right) \tag{1}$$

where γ is the surface energy of particles, κ is the curvature, and R_1 and R_2 are the principal curvatures. Fig. 3 shows the melting temperature of Cu NPs dependent on NP diameter and solid–liquid (S-L) interface energy. It is evident that the initial sintering temperature of metallic NPs decreases with the particle size. The smaller the particle size, the lower the corresponding initial sintering temperature. In the case of NPs sintering, the reduction in the initial sintering temperature can be understood as the lower melting temperature of nanoscale particles [45]. Generally, NPs paste, in which metallic particle size is below 100 nm in diameter, can form the dense structure at relatively low sintering temperatures (e.g., ≤300 °C), as shown in Tables III and IV. Once NPs form joints, they will possess higher melting temperatures, such as those of the bulk metal. Thus, reducing the particle size from the micrometer to the nanoscale range can

TABLE III
COMPARISON OF AG NPS PASTE SINTERING TECHNOLOGIES

Materials	Particle Size (nm)	Sintering Temp. (°C)	Sintering Pressure (MPa)	Sintering Time (min)	Precondition	Atmosphere	Shear strength (MPa)	Conductivity (μS/cm)
Ag NPs paste [39]	30	280	0	10	Temp. ramp (20 min)	Air	43	0.26
Ag NPs paste [40]	30–50	300	0	40	Temp. ramp (20 min)	Air	43	/
Ag NPs paste [56]		240	40	5	Preheat treatment at 270 °C for 3 h	Air	50	/
Ag NPs paste [66]	3–24	300	1, 5	5		Air	25–40	/
Ag NPs paste [67]	5, 10, 100	250	5	3		Air	30	/
Ag NPs paste [68]	<50	275	5	20	Four drying steps at 50, 75, 100, and 125 °C	Air	31.6	/
Ag NPs paste [69]	40	160~350	0, 5	5, 30	80 °C drying	Air	20@0 MPa; 50@5 MPa	/
Ag NPs paste [70]	<50	275	5	1	Predried for 30 min at 50 °C followed by 30 min at 125 °C	Air	40	/
Bimodal Ag NPs paste [71]	10, 50	250	0	30	Ultrasonic mixing of two types of unimodal Ag NPs	Air	41.80	/
Ag flakes paste [72]	80 nm thick. (8 μm dia.)	300	0.4	60		Air	23	/
Ag NPs paste [73]	50	280	0	10	Three-step drying at 50, 100, and 180 °C	1% O_2/N_2; N_2; 4% H_2/N_2.	35; 25; 45.	/
Ag flakes paste [77]	average size: 1.57μm	160	0	60			27	0.09

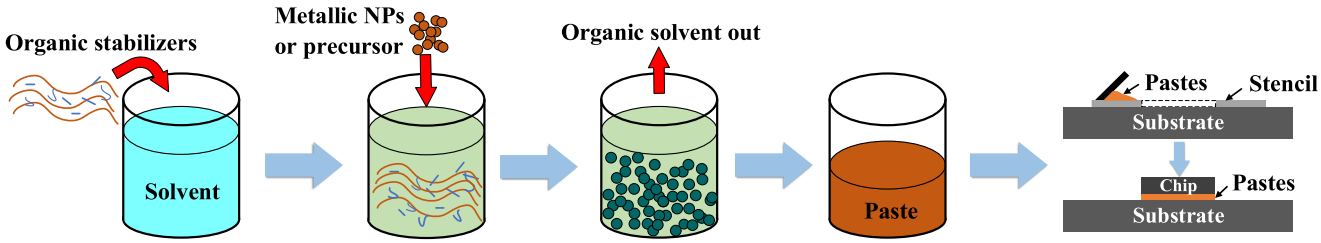

Fig. 4. General fabrication process of metallic NPs' pastes [46], [47], [48], [49].

lower the sintering temperature and help achieve better performance [41]. In this section, metallic NPs sintering materials and processes will be thoroughly surveyed.

A. Metallic NPs Sintering Materials

1) Metallic NPs Paste: Currently, Ag and Cu NPs are the primary sintering materials. Typically, the metallic NPs or precursors are mixed with organic solvents and additives to form metallic NPs paste [46], [47], [48], [49]. Typical synthesis routes for NPs include chemical reduction, laser ablation, mechanical ball milling, and supercritical fluid technology [10], [51]. These methods vary in terms of particle size distribution, oxidation state, and cost. The general pastes fabrication process is illustrated in Fig. 4. First, organic stabilizers and some special additives are selected and filled into a solvent. Second, metallic NPs are filled into the solvent and fully mixed with it. Third, a part of the organic solvent is dried out and each metallic NP

TABLE IV
COMPARISON OF CU NPS PASTE SINTERING TECHNOLOGY

Materials	Particle Size (nm)	Sintering Temp. (°C)	Sintering Pressure (MPa)	Sintering Time (min)	Pre-condition	Atmosphere	Shear strength (MPa)	Conductivity (μS/cm)
Cu NPs paste [84]	80	250	0.6	30	Formic acid treatment;	Ar	25	> 0.2
Cu NPs paste [85]	30	260	10	5	Formic acid treatment	5% H_2/N_2	43.4	0.18
Cu NPs paste [86]	50	200	0	30		N_2	39	0.0625
Cu NPs paste [87]	50	300	0.4	30	1.3 wt. % ascorbic acid treatment	N_2	24.8	/
Cu NPs paste [88]	60.5	300	1.08	60		5%H_2/Ar	31.88	0.09
Cu MP/NPs (40%:60% wt. %) paste [49]	70–200 Cu NPs 60% + 1–2 μm Cu MP 40%	200	0	15	Infrared dry at 70 °C for 1 h	Formic acid-activated N_2	19 ± 5	/
Cu NPs paste [89]	2–110, mean 40.4	300	5	/	/	Air	>13	0.012
Cu NPs paste [90]		240	10	3	Cured in an N_2 oven at 80 °C for 30 min	Air	28.1	/
Cu NPs paste [91]	50	220	0	5	Insitu reduction	Air	30	/
Cu NPs paste [92]		225	0	/		H_2	>40	/

is covered with a layer of organic shell. These organic shells can protect metallic NPs to prevent their aggregation, keep metallic NPs from oxidation, modify paste viscosity, etc. The organic stabilizers in the shell can stabilize unsaturated bonds between surface atoms of metal particles, thereby generating a stable metal NPs paste. Organic reducing agents, such as oxalic acid and formic acid, can effectively prevent oxidation of the metallic NPs during the preparation and sintering processes. Finally, the prepared paste is generally coated on the substrate by a stencil print, and the chip and substrate are bonded by a

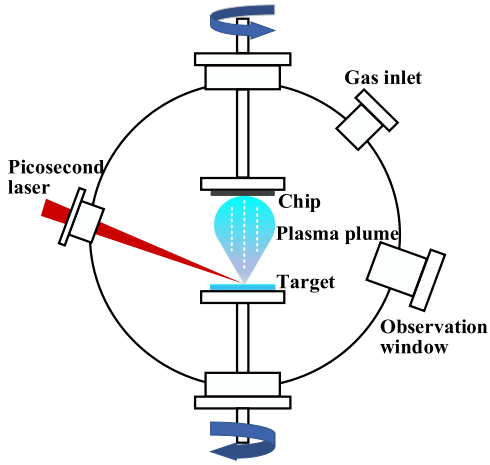

Fig. 5. Schematic diagram of PLD method [54], [55].

pressure-assisted or pressureless sintering process. Additionally, special treatments, such as the washing process and metallization, are required before the die attach [52].

2) Metallic NPs Deposition: Different from metallic NPs paste, which needs to be coated on the metalized surface, metallic NPs can be directly deposited on any target via physical vapor deposition (PVD) techniques, such as pulsed laser deposition (PLD) [53], [54]. Fig. 5 illustrates the schematic diagram of a PLD process. PLD involves four key steps, including laser ablation of the target material, ejection of the target material into the plasma plume, deposition of the plasma plume, and growth of NPs [53], [54], [55]. Laser ablation is primarily controlled by the pulsewidth or pulse duration [53]. The average size of NPs decreases rapidly with the reduction of laser pulse duration. Furthermore, the final morphology of NPs is influenced by the deposition atmosphere, substrate rotation, laser power, and deposition time. Jia et al. [55] deposited a supersaturated Ag-7.3 wt% Cu alloy NPs layer on the back side of the SiC die. The sintering process can be conducted in an air atmosphere without the assistance of a reduction agent. The shear strength can reach over 20 MPa when the bonding temperature reaches 300 °C. This method eliminates the use of organic compounds. And it also has the potential advantages of precise and easy control.

B. Metallic NPs Sintering Process

1) Heat-Press-Assisted Sintering: Metallic NPs sintering processes are generally classified as nonpressure and pressure-assisted types according to the absence or presence of applied pressure during the sintering process [56], [57]. Nonpressure and pressure-assisted sintering under a certain temperature is widely used now. Fig. 6 illustrates the schematic diagram of the NPs sintering process. Each NP is covered with an organic shell in the initial state, as shown in Fig. 6(a). During the sintering process, the organic shells are first released from the paste. The release involves two fundamental steps: the separation of the organic shells, which depends on their binding energy to the metallic NPs, and the evaporation of the shells, which is related to their inherent boiling point [58], [59]. Then, with supplied

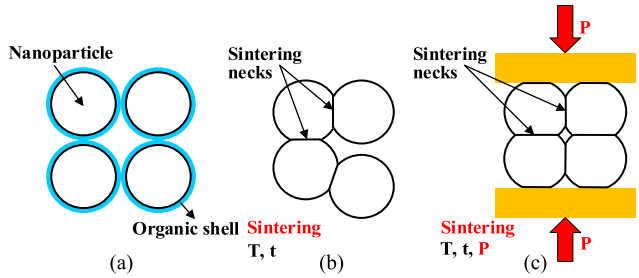

Fig. 6. Schematic of NPs sintering process. *T*, *t*, and *P* stand for sintering temperature, pressure, and time, respectively. (a) Initial state. (b) Nonpressure sintering. (c) Pressure-assisted sintering [38].

energy, usually heat and pressure, NPs can form sintering necks, as shown in Fig. 6(b) and (c). If appropriate pressure assistance is provided, NPs can achieve higher density and less-porosity joints, as illustrated in Fig. 6(c). The formation of the sintering neck follows the sintering process based on atomic surface diffusion: first, a contact area is formed, followed by the formation of necking through mass transportation [65]. This transition from the positive curvature of spherical particles to the negative curvature of the necking area reduces the total surface energy. Nonpressure sintering performed in a convection oven requires up to tens of minutes under a lower sintering temperature, while pressure-assisted sintering was relatively fast. Higher temperature and pressure could increase the densification rate, accelerate the metallic atom diffusion and bonding, increase the sintered bulk density, and, thus, significantly improve the properties of sintered metal. However, increasing temperature and pressure could destroy SiC power devices and other packaging materials. Higher pressure could also hinder the release of organic additives. Therefore, a suitable sintering parameter is necessary to be considered.

Molecular dynamics' studies were usually conducted to investigate the sintering mechanism [60], [61], [62], [63], [64]. During the heating process, as the sintering temperature rises, the energy of the entire system increases, and the interaction among atoms becomes stronger. During the isothermal holding process, the temperature no longer changes, and the potential energy tends to stabilize, gradually stabilizing the system. The initial formation mechanism of sintering necks between NPs mainly relies on vertical atomic diffusion, while the further enlargement mechanism of sintering necks is mainly caused by horizontal atomic diffusion. In the later stages of sintering, viscous flow is the main mode of atomic migration, which tends to be horizontal rather than vertical motion [60]. At this stage, the contribution to atomic displacement mainly comes from atoms far from the sintering neck, whereas, in the early stages of sintering, it primarily comes from the sintering neck region. The displacement distance of atoms continues to increase until the end of sintering.

Furthermore, phase transition analysis shows that, during the sintering process, atomic rearrangement recrystallization could occur in the sintering neck region and its vicinity [60], [61]. For sintered Cu, as sintering progresses, first, the initial face-centered cubic (FCC) atoms in the sintering neck region could

transform into amorphous atoms or hexagonal close-packed (HCP) structures, accompanied by the formation of dislocations and stacked faults. In the subsequent sintering, the total length of dislocations gradually decreases, and recrystallization of the amorphous structure occurs, ending the plastic deformation in the sintering neck region. Finally, twin boundaries spanning two NPs form, creating a relatively stable crystalline structure. In pressure-assisted sintering, applying pressure to the NPs could change the dominant coalescence kinetics from slight surface diffusion to intensive volume diffusion and plastic flow driven by the defects. Therefore, higher sintering pressure may lead to a greater degree of NP aggregation [61].

1) Ag NPs sintering

Table III summarizes some typical low-temperature sintering conditions and mechanical performance of most-used Ag NPs' pastes. As shown in Table III, the commonly used sintering temperature, pressure, and time ranges are 250–300 °C, 0–5 MPa, and 5–30 min, respectively. Preconditioning is a necessary step for most of the sintering methods. The shear strength of the sintered joints is above 25 MPa. Thermal conductivity can reach up to 278 W/m·K [71]. The sintering time, pressure, and temperature form a delicate balance [74], [75]. Typically, a decrease in one or two parameters (e.g., temperature) requires an increase in the others (e.g., pressure) to compensate for achieving similar joint strength [40], [66], [67], [68].

Researchers have also studied nanoflakes (flake-shaped NPs), which can induce denser microstructures compared with spherical NPs [76], [77], [78], [79], [80], [81]. Li et al. [77] achieved low-temperature sintering at 160 °C using solvent and interface engineering, resulting in a joint strength of 27 MPa. Solvents with high wetting properties can generate high capillary adhesion between the Ag flakes and the substrate, ensuring tight contact. However, the sintering time was long, taking 60 min. Nanoflakes with sizes ranging from 40 to 260 nm were sintered at 300 °C, resulting in a high-performance sintered Ag joint with a porosity of 5.1%, shear strength of 49.8 MPa, and electrical conductivity of 31.6 $\mu\Omega$·cm [78]. Generally, higher curvature tends to promote faster sintering kinetics, while the large flat surface of nanoflakes may result in slow sintering kinetics. However, the average neck shrinkage size of nanoflakes is thicker than that of spherical NPs [76]. This controversial result shows that the nanoflakes paste has a unique sintering mechanism that cannot be explained by traditional diffusion necking growth models. Nanoflakes have sharp corners where the diffusion-potential gradient is large and bonds are unsaturated, leading to a tendency for diffusion to reduce surface energy. Therefore, the corners of nanoflakes begin to shrink and become rounded first during sintering.

Fig. 7(a) illustrates the results of molecular dynamics' simulations. As temperature rises, the atomic movements are predominantly concentrated at the four corners of the nanoflakes. Most of the atoms located at corners moved along the surface and edge or inward into the bulk, gradually rounding the sharp corners of the nanoflakes. Subsequently, the edges of nanoflakes deform at higher temperatures, as shown in Fig. 7(b) and (c). As the temperature rises, the solvent rapidly evaporates, causing a reduction in the gaps between the nanoflakes. As the

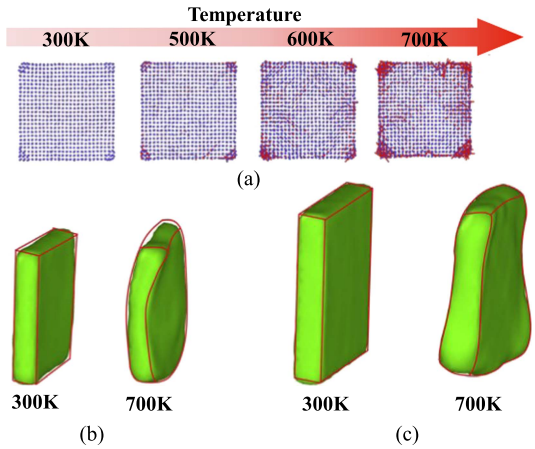

Fig. 7. (a) Displacement vector of nanoflakes from 300 to 700 K. Shape changes of nanoflakes with different sizes during sintering: (b) 5 nm and (c) 7 nm [79].

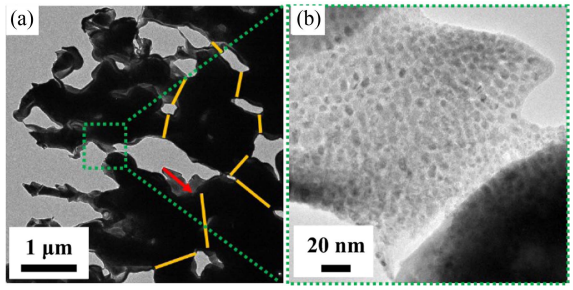

Fig. 8. (a) Transmission electron microscopy (TEM) images of the nanoflakes' pastes after sintering under an air atmosphere at 250 °C for 10 min. (b) Magnified view. Necking size is indicated by the yellow line. The large necking is indicated by a red arrow [76].

temperature increases and the sintering process progresses, the deformed portions of closely packed nanoflakes undergo mutual diffusion at the interfaces. This diffusion primarily occurs at three critical regions: corners, corners and edges, and edges and edges. These interactions contribute to the formation of a dense and continuous interconnecting structure, enhancing the overall integrity and mechanical strength of the material. It is noteworthy that the generation of some small spherical NPs is detected during the sintering process [76], as shown in Fig. 8. As NPs are thermodynamically unstable, the crystal growth of agglomerating NPs accelerates the networking between the particles, contributing to the fast-necking growth. The NPs created diffusion paths by bridging between nanoflakes, expediting the sintering process. The origin of NPs may be attributed to the initial microstrains caused by high dislocation density in the grain boundaries of nanoflakes and subsequent strain relaxation during heating.

2) Cu NPs sintering

It is noted that the sintered Ag NPs have severe electromigration (EM) issues in high-current applications (e.g., 1×10^4 A/cm^2, 200 h, 150 °C) [82], [83]. Cu has similar thermoelectrical properties with Ag but higher resistance to EM. Cu NPs

paste has become one of the emerging die-attach materials in high-temperature and high-power electronics. Table IV summarizes the low-temperature sintering conditions and mechanical performance of the most-used Cu NPs' pastes. From Table IV, the commonly used sintering temperature, pressure, time, and particle size ranges are 200–300 °C, 0–10 MPa, 3–30 min, and below 100 nm, respectively. Reductive treatment and a protective atmosphere are necessary steps for most sintering methods. The shear strength of sintered joints is above 20 MPa, the electrical conductivity is less than 100 $\mu\Omega$·cm, and the thermal conductivity can reach 180 W/mK [92]. The selection of organic additions in the paste formulation determines the range of sintering temperatures [10]. Applying the pressure can promote Cu atom diffusion, thus reducing voids within the sintered Cu at the interface. The particle size affects the total surface energy of particles, which determines the strength of the sintering driving force. For example, reducing particle size and increasing the sintering pressure, even with a shorter time, can still significantly increase the shear strength [84], [85]. Some special paste formulations can achieve higher shear strength even at a low sintering temperature and nonpressure condition [86], [87]. Additionally, preparing mixed-particle pastes is also an effective choice for higher sintering density [49]. In theory, the maximum packing density for the same size NPs is approximately 74% before sintering, achieved in an FCC or HCP [64]. To further enhance packing density, microparticle (MP)/NP hybrid metallic pastes can be used for sintering. The incorporation of nanoscale metallic particles can effectively fill the pores between micron-sized particles, thereby enhancing the packing density of the particles [49]. The increase in packing density also comes with another benefit: a reduction in the content of organic. It should be noted that an increase in the proportion of MP typically accompanies a rise in sintering temperature to attain more thorough sintering [36]. Therefore, the ratio of MP/NP needs to be adjusted as per specific requirements.

However, Cu NPs are easily oxidized in the air atmosphere during the sintering process. The air atmosphere induced some voids, and the bonding layer was less dense than in the vacuum atmosphere [93]. Therefore, antioxidation methods are usually used, such as protective atmosphere, reducing gas, and acid pretreatment. Vacuum or inert gas (Ar, N_2, etc.) is the most common protective atmosphere, but existing oxidation cannot be removed. Therefore, a reduced atmosphere is required. For instance, the formic acid-enriched N_2 atmosphere can be made by bubbling nitrogen (gas) into a formic acid (liquid) [94]. Formic acid in N_2 can reduce Cu oxidation before and during sintering. As shown in Table IV, some other reducing atmospheres are also used, such as 5% H_2/N_2, to reduce oxide generation. In addition, pretreatment of the paste with a reducing agent before sintering is also a commonly used method. Fig. 9 illustrates the schematic diagram of the Cu-Cu joint process using formic acid pretreatment. The chemical reaction equations of the CuO and formic acid are shown as (2) and (3). After formic acid treatment, the sintered layer shows a more coarsened reticulated structure and better bonding with the Cu pad. In addition, longer treatment time may lead to Cu reoxidation, thereby hindering the sintering process [85]. Therefore, formic acid treatment time should be strictly controlled

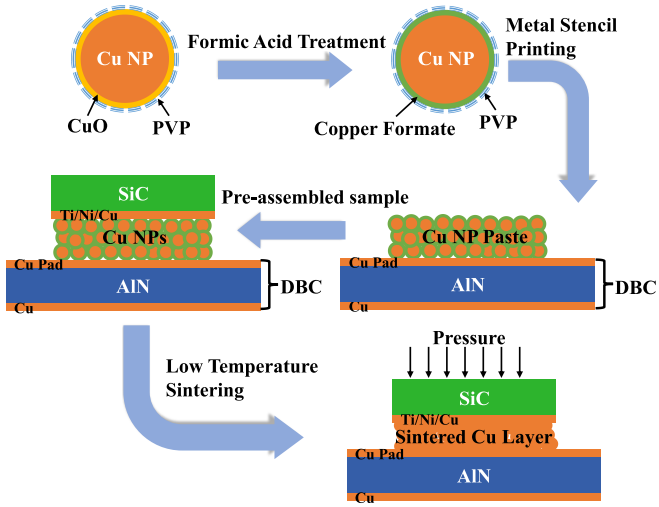

Fig. 9. Schematic of Cu-Cu joint process using formic acid pretreatment [85].

$$\mathrm{CuO} + 2\mathrm{HCOOH} \rightarrow \mathrm{Cu(COOH)_2} + \mathrm{H_2O} \quad (2)$$

$$\mathrm{Cu(COOH)_2} \rightarrow \mathrm{Cu} + \mathrm{CO_2} + \mathrm{H_2}. \quad (3)$$

However, the Cu NPs sintering process in a protective or reducing gas atmosphere is complicated and costly, especially in industrial applications. Cu NPs sintering in an air atmosphere is a more potential technology. Jianfeng et al. [89] successfully realized the low-temperature sintering of Cu NPs in an air atmosphere by incorporating polyvinylpyrrolidone (PVP) into the Cu NPs paste. PVP acts as a protective coating material on the NPs, as shown in Fig. 10, preventing oxidation during the heating process. The shear strength was 13 MPa at temperatures above 220 °C.

Similarly, the Cu-Ag core-shell NPs paste can be sintered in an air atmosphere. The Cu-Ag core-shell NPs are made by mixing preprepared Cu NPs with Ag compound and allowing them to react [95], [96]. The Ag shell can prevent the oxidation of Cu NPs during sintering in the air. However, the cost of the core-shell structure method is significantly higher than pure Cu NPs, and the complex synthesis process is also a potential challenge. Zuo et al. [91] achieved sintering in the air through an in situ reduction method. The Cu atoms inside Cu NPs were protected by oxide shells, allowing the particles to achieve sintering while simultaneously undergoing reduction.

In addition, the sintering temperature, sintering time, and other parameters of Cu NPs paste can be determined by material characterization experiments, e.g., thermogravimetric analysis (TGA), elevated-temperature X-ray diffraction (XRD), and differential scanning calorimetry [55], [66], [85], [88]. Zhang [90] analyzed the sintering behavior of commercial Cu NPs' pastes by TGA and XRD experiments and realized the Cu NPs sintering in an air atmosphere. Fig. 11 compares the mass of Cu NPs paste dependent on temperature in Ar and compressed air. Fig. 12 shows the XRD patterns of Cu NPs paste at various elevated temperatures. From the two figures, the Cu oxidation starts to increase slowly, and the decomposition of organic compounds

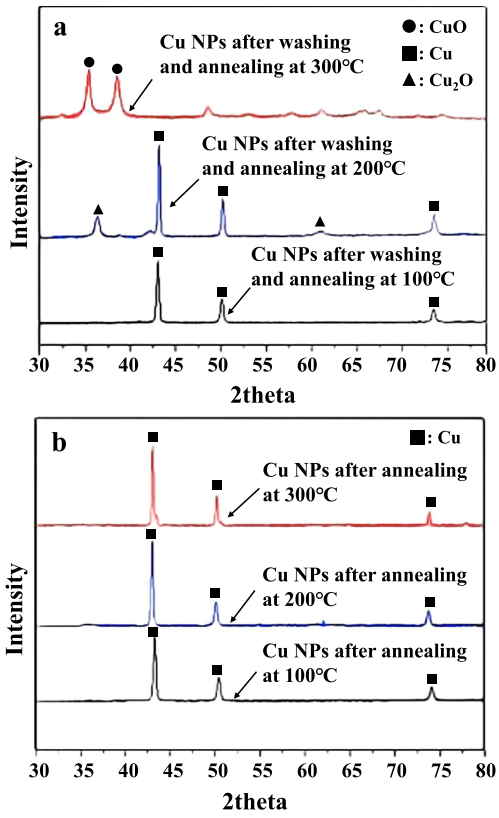

Fig. 10. XRD patterns of Cu NPs after annealing. (a) Cu NPs without thick PVP protection (after washing with deionized water). (b) Cu NPs with thick PVP protection (without washing) [89].

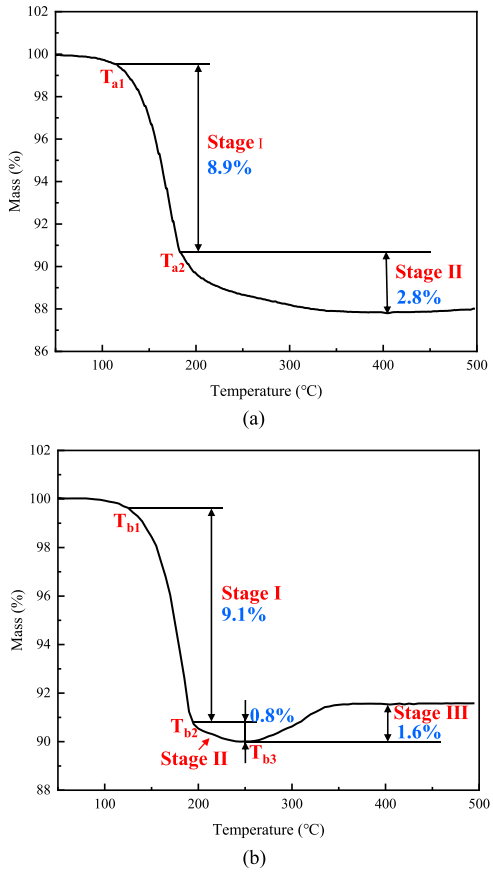

Fig. 11. TGA results of the Cu NPs paste. (a) In Ar. (b) In compressed air [90].

further slows down, but the mass continues to decrease. After T_{b3}, the mass increase caused by oxidation exceeds the mass decrease caused by the release of organic compounds, leading to an overall increase in mass. Therefore, the sintering temperature can be selected between T_{b2} and T_{b3}. It is worth noting that a small amount of oxidation is observed within the bonding layer after sintering. However, if it does not affect the sintering process and long-term reliability of sintered joints, partial oxidation is acceptable.

2) Current- and Laser-Assisted Sintering: The heat-press-assisted sintering method is relatively complicated, time-consuming, and sometimes requires inert gas atmospheres [16]. In addition, there are some other sintering technologies, such as current-assisted sintering and laser-assisted sintering [96]. These sintering methods provide an alternative way of supplying heat source. In [97], [98], [99], and [100], a rapid current-assisted sintering technology was used to bond electronic devices with Ag NPs paste. The sintering schematic is shown in Fig. 13. The shear strength increases with the current and time. At a current of 8.25 kA and a sintering time of 1 s, the shear strength of the sample approaches 100 MPa. Pressure assistance can improve the contact between the substrate and the Ag NPs paste, preventing voids or cracks generated during the sintering process due to gas release. It is noted that applying current to extremely thin bonding regions is a challenge in the actual production. Further research is needed to investigate whether high currents can cause damage to the chip. Besides, exploration has also been conducted on laser-assisted rapid sintering processes for chip interconnection using Ag NPs' pastes [101], [102]. The sintering schematic is shown in Fig. 14. The results indicated that the laser-assisted sintering could significantly shorten the time, and the sintering process can be finished within 1 min. The Si chip absorbs the laser beam, generating localized heating effect, which can increase the temperature of the Ag NPs paste and enable the bonding of Si-Ag-DBC. The shear strength increases with the laser power, load, and sintering time. In addition, laser-assisted sintering offers extremely short sintering time and high cooling rates, which helps to reduce residual stress and oxidation effects [102]. Due to the fast-sintering time, the sintered Cu NPs could reach good performance in an air atmosphere by laser-assisted sintering technology.

C. Interface and Reliability

As the die-attach layer in the power electronic packaging, sintered metals are often subjected to various loads and stresses, with shear being the most common [10]. Shear strength, which is easy to measure and intuitive, is often used to characterize the performance of sintered joints. The strength of sintered joints is determined not only by the sintered material itself but also by the interface strength between the sintered metal and the substrate. In other words, shear strength is controlled by both the sintering process (e.g., time, pressure, temperature, particle

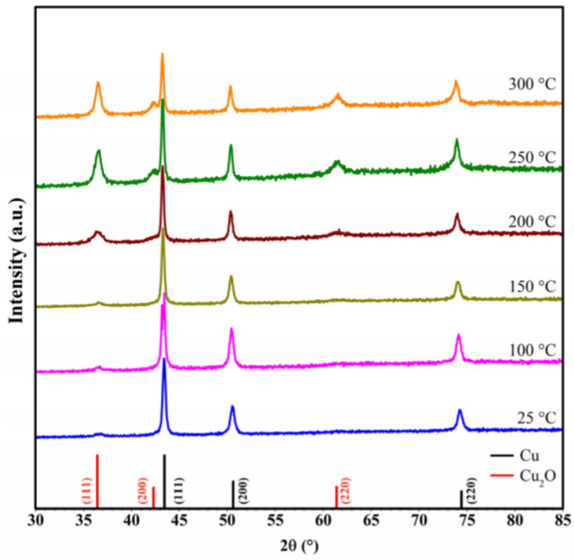

Fig. 12. XRD scans of the Cu NPs paste at elevated temperatures in air [90].

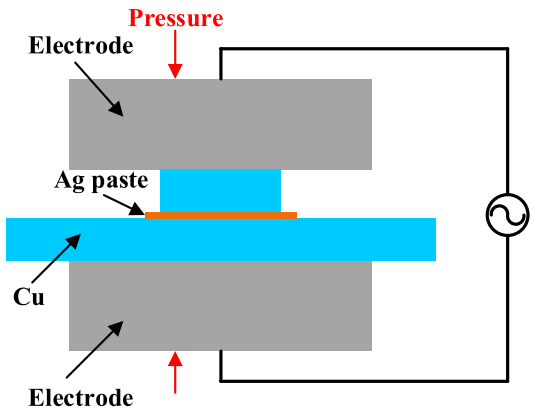

Fig. 13. Schematic illustration of the current-assisted sintering technology [97], [98], [99], [100].

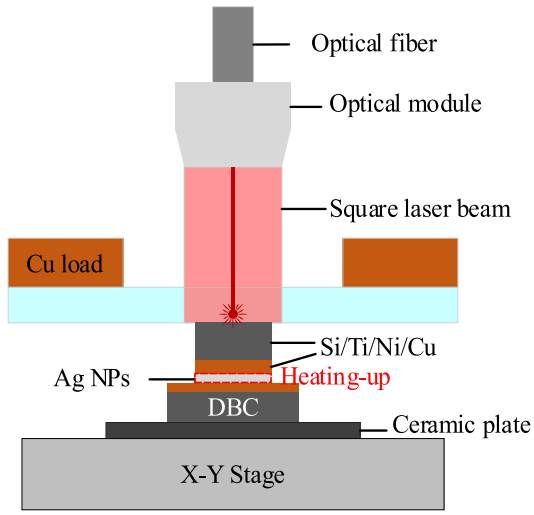

Fig. 14. Schematic illustration of the laser-assisted fast Ag-based NPs paste sintering [102].

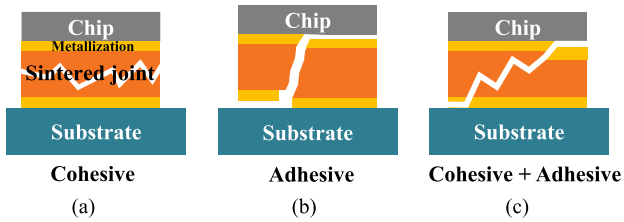

Fig. 15. Different fracture modes after shearing [103], [104].

morphology, and sintering atmosphere) and the substrate (e.g., metallization). After shearing, failure modes can generally be divided into three categories: cohesive, adhesive, and cohesive–adhesive, as shown in Fig. 15. Cohesive failure occurs within the sintered metal, indicating that the metallic NPs have not formed strong long-range connections. Pressure-assisted sintering can significantly reduce the occurrence of such failures. Adhesive failure occurs at the interface between the sintered metal and the metallization layer, and fracture between the metallization layer and the substrate has also been observed [103]. Therefore, selecting the appropriate metallization is crucial for obtaining excellent sintered joints.

Typically, sintered Ag can form great joints on Au, Ag, or Cu metallization layers. For Cu and Ni metallization, sintered Cu can typically form higher bonding strength and reliability compared with sintered Ag [10], [105]. This phenomenon may be due to the matching of lattice constants at the contact interface. The underlying substrate metallization layers act as seed crystals for sintered Cu, promoting Cu growth and facilitating interconnection at the interface [106], [108]. Additionally, some researchers suggest that the absence of a significant Kirkendall effect may also be one of the reasons, a finding supported by both experiment and molecular dynamics' simulations [110], as shown in Fig. 16. When Cu NPs are sintered on Ni or Cu metallization layers, the interdiffusion is weak, and no significant voids distribution is observed at the sintering interface, resulting in stronger joints.

Compared with Ni or Cu metallization, the interdiffusion coefficients between the sintered Cu layer and Au or Ag metallization layers are significantly higher by 2–3 orders of magnitude [110]. The interface exhibits pronounced interdiffusion, as illustrated in the molecular dynamics' simulations in Fig. 16(b). Studies have shown that, during sintering, the Kirkendall effect can create large voids in the interface between the sintered Cu layer and metallization layers, resulting in weaker joint strength [110]. Experimental data about the distribution of porosity content in sintered Cu layers are shown in Fig. 16(a). It can be observed that Au and Ag metallization exert a strong influence on the adjacent sintered Cu, although this influence diminishes with increasing distance from the metallization layer. Additionally, Ishikawa et al. [109] reported that, for the Au metallization, the shear strength decreased with the sintering temperature. Large voids were observed beneath the Au metallization layer. The metallization layers were typically prepared using electroplating or sputtering techniques. However, some research suggests that for standard finishing layers prepared by chemical

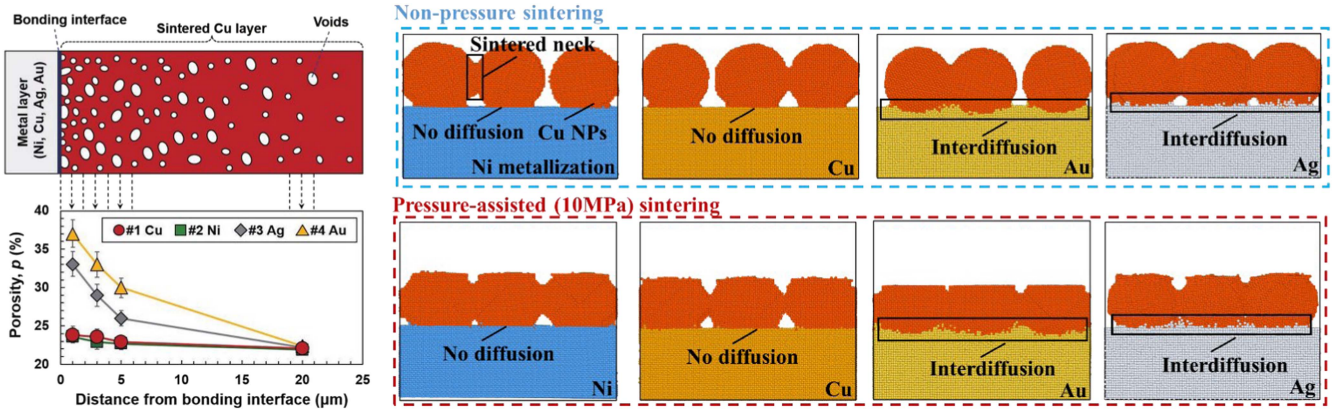

Fig. 16. (a) Porosity of sintered Cu on the different metallization layers [110]. (b) Molecular dynamics simulation of interdiffusion at the interface between Cu, Ni, Au, and Ag metallization layers and sintered Cu.

plating [e.g., electroless nickel immersion gold (ENIG)], the Au metallization can enhance shear strength and reliability [94], [111]. Researchers believe that the formation of IMCs resulting from the interdiffusion between sintered Cu and the ENIG layer enhances joint strength.

However, in another study by Nakako et al. [92], high shear strength sintered Cu joints (>40 MPa) were achieved on Cu, Ni, Au, Ag, and Pd metallization layers. Cu joints exhibited superior thermal reliability compared with Ag joints after 1500 temperature cycles (−40 °C to 200 °C). For other metallization layers, such as Ti, Mn, and Cr, the formation of stable oxides at the interface, due to their lower standard free energy of oxide formation, significantly reduced shear strength [107]. These findings illustrate that the influence of metallization on joint strength depends not only on intrinsic properties but also on factors, such as fabrication processes.

After reliability testing, traditional solder (e.g., Sn-based solder) often shows a decrease in joint strength, especially for SiC device packaging [112]. Studies have indicated that metallic NPs sintering shows excellent reliability in power cycling, thermal cycling, and thermal shock [92], [109], [110], [113], [114], [115], [116]. Sintered Cu demonstrates a longer lifetime than sintering Ag in power cycling [10], [105]. Sintered Cu showed no changes after 550 000 power cycles, while sintered Ag broke down after only 220 000 cycles when tested at a low junction temperature of 25/175 °C [105]. The enhanced reliability of sintered Cu is primarily attributed to its higher yield strength and lower CTE mismatch [105]. Tested at 25/200 °C, no obvious change in the thermal conductivity of sintered Cu joint was observed after 1000 power cycles by thermal transient tester technology [113], [114]. Obvious lateral cracks were observed in the sintered Cu joints using short carbon chain capping agent cappers after only 360 cycles when tested at a low junction temperature of 65/250 °C. On the other hand, sintered Cu joints using long carbon chain capping agents showed only the generation of vertical cracks after 3000 cycles [115], [116], [117]. Vertical cracks have a minor impact on the thermal conduction path, resulting in minimal changes in the maximum junction temperature. However, lateral cracks can significantly impede heat flow conduction. The occurrence of lateral cracks has been attributed to the insufficient steric hindrance effect of the short carbon chain capping agent to prevent the aggregation of NPs, leading to the formation of large Cu NPs and reducing the sintering driving force [10], [117].

In contrast to the traditional solder, sintered Cu shows an increase in shear strength when subjected to thermal cycling or thermal shock test [113], [114]. Compared with vacuum environments, sintered Cu joints showed higher shear strength after thermal shock in the air. Therefore, researchers attribute the increase in shear strength to the formation of Cu oxides, which create a denser structure and potentially improve bonding strength [114]. In contrast, sintered Ag joints showed peeling-off at the edges after 1000 temperature cycles, with the damage gradually spreading with increasing cycles [92]. After thermal shock, small cracks may appear at the edges of the bond layer due to the CTE mismatch. However, these small cracks have minimal effect on the shear strength [113]. In addition, the common failure mode of the adhesive layer is propagation from the edges to the interior after the reliability test [112], [114].

IV. Challenges and Outlook of Cu NPs Sintering

Currently, sintered Ag has become a relatively mature technology with excellent thermal and electrical conductivity properties. Ag NPs sintering technologies have been used in many power modules. However, sintered Ag is prone to serious EM in high-current operating environments, often requiring specific optimization measures for practical applications. In comparison, sintered Cu offers similar thermal and electrical properties to sintered Ag and performs better in high-current environments. The sintered Cu is a promising die-attach material. However, there are still some key issues to be solved. Some challenges and outlooks are discussed as follows.

A. Challenges of Cu NPs Sintering

1) Cu Easy Oxidation in the Sintering Process: Cu easy oxidation has been a big issue during the sintering process, which may lead to a poor bonding strength, thus limiting the rapid

application of Cu NPs paste in the industry. To avoid or reduce the Cu oxidation in the sintering process, a protective atmosphere (e.g., N_2 and Ar) or a reductive atmosphere (e.g., H_2 and formic acid) is usually used. Sometimes, a preconditioning process is needed. In all, the sintering process of Cu NPs paste is relatively complicated compared with the Ag NPs sintering process, and Cu NPs sintering in an air atmosphere is a challenge. Except for selecting appropriate organic additives, the sintering temperature should be confirmed based on thermal gravity experimental results in the air atmosphere, as shown in Fig. 11. In addition, the core-shell structure offers an innovative approach to enhance the sintering process of Cu NPs in an air environment. Through a preoxidation and reduction process, a protective shell that can thermally decompose back into Cu is formed on the surface of Cu NPs. During sintering, the shell decomposes and forms sintering necks while protecting the internal Cu atoms. Further exploration of processing techniques and mechanistic research is still needed.

2) Tradeoff Among Thermal, Electrical, and Mechanical Properties: In the SiC power module, the die-attach layer is supposed to act as a buffer layer except for interconnecting the die and the substrate. As the heat flux of SiC devices increases, the die-attach layer should have much higher thermal and electrical conductivity. This requires the sintered Cu to have the lowest possible porosity [74]. As a sintering metal, the theoretical limitations of sintered Cu properties can approach those of the bulk Cu. However, low porosity can lead to high Young's modulus, which could make the die crack [74]. The maximum principal stress of the die would increase with the modulus of the die attach. Higher Young's modulus is adverse to the mechanical performance of SiC devices. Therefore, tradeoff design that simultaneously considers electrical, thermal, and mechanical performances is a challenge. Multiobjective optimization is essential.

3) Inherent Effects of Pressure, Temperature, and Time: Nonpressure and pressure-assisted sintering are the two main sintering techniques for Cu NPs paste. Applied pressure, sintering temperature, and holding time would affect the final state of Cu NPs paste, as shown in Fig. 6. Increasing the pressure, raising the temperature, and extending the time can promote NPs sintering and the sintered Cu has excellent performance. However, if the process condition is not properly, its performance will be far below the expectation. Moreover, a higher pressure could damage the die, a higher temperature could induce higher stress on the die corner after sintering due to the high-temperature difference and CTE mismatch between the die and the substrate, and the sintering efficiency over a longer time is lower. Therefore, it is essential to thoroughly understand the inherent effects of pressure, temperature, and time on Cu NPs sintering.

B. Outlook of Cu NPs Sintering

Due to the excellent performance, Cu NPs sintering technology will be widely used in power electronics and microelectronics not only in attaching the die but also in the lid, heat sink, etc. For a relatively complicated package or module, several types of solders with different melting temperatures are usually selected. The process procedure is based on the melting temperature of solders and reflows from high-to-low temperatures. Moreover, different types of solders require different surface metallization, and high reflow temperatures would induce high stress on the component corner, thus leading to cracks or delamination. The characteristic of "low-temperature sintering, high-temperature service" of NPs Cu sintering can effectively address this issue, as shown in Fig. 17. After sintering, the melting point of the bond layer is close to that of bulk Cu, which ensures that the bonded layer will not melt during subsequent heating bonding processes. Multiple steps of Cu NPs sintering are promising for replacing multiple reflows of solders based on their melting temperature.

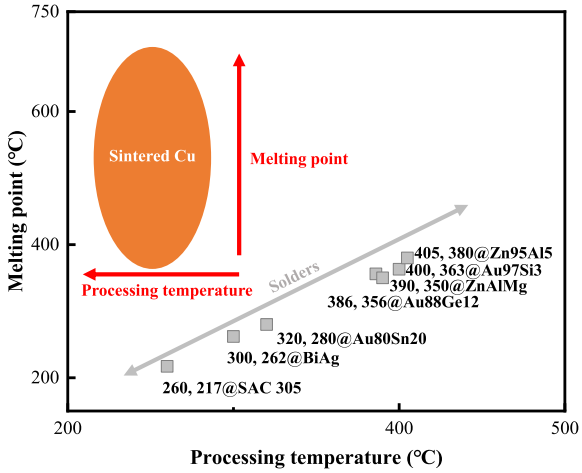

Fig. 17. Estimated processing temperature and melting point for solder and sintered Cu.

In addition, as the SiC die size tends to be smaller in comparison with the Si counterparts, the current density and heat flux through the die attach are increasing rapidly. High current density can pose the risk of severe EM, forming voids and reducing mechanical and electrical behavior. High heat flux can lead to hotspots inside devices, reducing the performance and increasing the risk of failure. This means that the die attach needs to have high thermal conductivity to conduct the heat generated by the chip. Compared with sintered Ag, sintered Cu possesses similar thermal and electrical conductivity. Moreover, sintered Cu can work well in high-temperature, high current density environments without causing EM issues. Sintered Cu as a die-attach material has shown increasing advantages and has significant application value.

V. Conclusion

With the motivation of fully utilizing SiC devices' performance of the high temperature, some conventional high-temperature die-attach materials, such as solders and TLP bonding materials, were first reviewed. As the SiC die size tends to be smaller in comparison with the Si counterparts, its heat flux can reach up to 1 kW/cm^2 or beyond. Such high heat flux cannot be quickly dissipated via the conventional die-attach materials. Their thermal conductivities are generally lower. Metallic NPs

sintering is a promising bonding technology due to its excellent physical properties and the features of low-temperature bonding and high-temperature service. Ag and Cu NPs sintering technologies were thoroughly reviewed. Some conclusions are drawn as follows.

1) Temperature (or temperature curve), pressure, and time are direct variables for optimizing the mechanical, electrical, and thermal properties of the sintered metal. An increase in temperature and pressure means a higher densification rate. The longer the sintering time, the denser the sintered metal becomes. However, the limits that the chip can withstand also need to be considered to prevent damage from sintering. In addition, some properties of the sintered metal are mutually exclusive. Higher electrical conductivity, thermal conductivity, and shear strength mean a higher stress on the die corner. Therefore, multiobjective optimization needs to be done.
2) The formulation of the paste and the particle size also have a significant impact on the sintered results. Particle size affects the total surface energy of the particles, which determines the strength of the sintering driving force. Organic additions in the paste have various specialized functions, such as viscosity control, reduction, and protection. These special functionalities will influence the printing of the paste and the behavior of metal NPs before and after sintering.
3) The cost of sintered Cu depends more on the preparation of Cu NPs (e.g., chemistry synthesis and PVD), paste formation, sintering process development, etc. So far, the cost of sintered Cu is still relatively high. Different sintering processes and paste formulations have been explored to decrease the cost, such as using commercially available Cu particles to prepare pastes and TGA analysis sintering methods.
4) Cu NPs easy oxidation is the primary problem that needs to be solved during the sintering process. Common methods to prevent oxidation include applying a protective or reducing atmosphere, or a combination of both, during sintering. However, these methods increase the complexity and cost of the process, especially in industrial production. The Cu NPs sintering in an air atmosphere is a more potential technology. Methods, such as core-shell protective structures, in situ reduction sintering, and TGA, have been explored and have shown promising results. The core-shell protective structures and in situ reduction sintering process are relatively complex but offer better versatility. As an analytical technology, TGA can simply achieve sintering in air with the suitable paste formula and cut costs. However, during the sintering process, a small amount of oxidation is inevitably generated. It needs to be controlled within an acceptable range that does not affect the performance and long-time reliability.
5) Some other sintering technologies, such as ultrasonic-, current-, and laser-assisted sintering, have been explored. Ultrasonic-assisted sintering can promote the occurrence and growth of the sintering neck. Current- and laser-assisted sintering provides an alternative way of supplying energy sources. The extreme-short sintering time can greatly improve production efficiency.
6) An excellent sintered joint requires both sufficient sintering and the appropriate metallization. Sufficient sintered metallic NPs not only can achieve excellent electrical, thermal, and mechanical properties but also show high reliability in temperature cycling, power cycling, and other tests. Failure at the interface between the metallization layer and the sintered layer has been observed. The influence of the metallization layer depends not only on its physical properties but also on factors, such as fabrication processes. Some metallization layers, such as Cu, Ni, Au, and Ag, have been proven to achieve good interconnection joints. Compared with Au and Ag metallization layers, Cu and Ni seem to perform better.

REFERENCES

[1] F. Hou et al., "Review of packaging schemes for power module," *IEEE J. Emerg. Sel. Topics Power Electron.*, vol. 8, no. 1, pp. 223–238, Mar. 2020.

[2] J. Millán, P. Godignon, X. Perpiñà, A. Pérez-Tomás, and J. Rebollo, "A survey of wide bandgap power semiconductor devices," *IEEE Trans. Power Electron.*, vol. 29, no. 5, pp. 2155–2163, May 2014.

[3] C. Neeb, L. Boettcher, M. Conrad, and R. W. De Doncker, "Innovative and reliable power modules: A future trend and evolution of technologies," *IEEE Ind. Electron. Mag.*, vol. 8, no. 3, pp. 6–16, Sep. 2014.

[4] T. Suzuki et al., "Macro- and micro-deformation behavior of sintered-copper die-attach material," *IEEE Trans. Device Mater. Rel.*, vol. 18, no. 1, pp. 54–63, Mar. 2018.

[5] N. Heuck et al., "Analysis and modeling of thermomechanically improved silver-sintered die-attach layers modified by additives," *IEEE Trans. Compon., Packag. Manuf. Technol.*, vol. 1, no. 11, pp. 1846–1855, Nov. 2011.

[6] L. A. Navarro et al., "Thermomechanical assessment of die-attach materials for wide bandgap semiconductor devices and harsh environment applications," *IEEE Trans. Power Electron.*, vol. 29, no. 5, pp. 2261–2271, May 2014.

[7] H. Zhang, J. Minter, and N.-C. Lee, "A brief review on high-temperature, Pb-free die-attach materials," *J. Electron. Mater.*, vol. 48, no. 1, pp. 201–210, Jan. 2019.

[8] V. R. Manikam and K. Y. Cheong, "Die attach materials for high temperature applications: A review," *IEEE Trans. Compon., Packag. Manuf. Technol.*, vol. 1, no. 4, pp. 457–478, Apr. 2011.

[9] K. S. Siow, ed., *Die-Attach Materials for High Temperature Applications in Microelectronics Packaging: Materials, Processes, Equipment, and Reliability*. Berlin, Germany: Springer, 2019.

[10] T. F. Chen and K. S. Siow, "Comparing the mechanical and thermal-electrical properties of sintered copper (Cu) and sintered silver (Ag) joints," *J. Alloys Compounds*, vol. 866, Jun. 2021, Art. no. 158783.

[11] H. Beyer, V. Sivasubramaniam, M. Bayer, and S. Hartmann, "Reliability of lead-free large area solder joints in IGBT modules with respect to passive and active thermal cycling," in *Proc. 9th Int. Conf. Integr. Power Electron. Syst.*, 2016, pp. 1–6.

[12] A. A. Bajwa, Y. Qin, R. Reiner, R. Quay, and J. Wilde, "Assembly and packaging technologies for high-temperature and high-power GaN devices," *IEEE Trans. Compon., Packag. Manuf. Technol.*, vol. 5, no. 10, pp. 1402–1416, Oct. 2015.

[13] J. Liu, W. Lv, Y. Mou, Y. Peng, F. Zhu, and M. Chen, "Sn-enhanced high-temperature reliability of Cu/nano-Ag/Cu joint via transient-liquid-phase bonding," *J. Mater. Sci.*, vol. 58, no. 26, pp. 10870–10884, Jul. 2023.

[14] M. V. Uvarajan, L. H. Lim, M. H. Goh, F. L. Ng, and W. C. Pan, "Temperature cycling aging studies of Zn-based solders for high-temperature applications," in *Proc. IEEE 17th Proc. IEEE Electron. Packag. Technol. Conf.*, 2015, pp. 1–5.

[15] H. Kang, A. Sharma, and J. P. Jung, "Recent progress in transient liquid phase and wire bonding technologies for power electronics," *Metals*, vol. 10, no. 7, Jul. 2020, Art. no. 934.

[16] H. Zheng, D. Berry, J. N. Calata, K. D. T. Ngo, S. Luo, and G.-Q. Lu, "Low-pressure joining of large-area devices on copper using nanosilver paste," *IEEE Trans. Compon., Packag. Manuf. Technol.*, vol. 3, no. 6, pp. 915–922, Jun. 2013.

[17] S. W. Yoon, K. Shiozaki, and T. Kato, "Double-sided nickel-tin transient liquid phase bonding for double-sided cooling," in *Proc. IEEE Appl. Power Electron. Conf. Expo.*, 2014, pp. 527–530.

[18] H. A. Mustain, W. D. Brown, and S. S. Ang, "Transient liquid phase die attach for high-temperature silicon carbide power devices," *IEEE Trans. Compon. Packag. Technol.*, vol. 33, no. 3, pp. 563–570, Sep. 2010.

[19] S.-E. Jeong, S.-B. Jung, and J.-W. Yoon, "A study of the growth rate of Cu-Sn intermetallic compounds for transient liquid phase bonding during isothermal aging," in *Proc. IEEE 20th Electron. Packag. Technol. Conf.*, 2018, pp. 225–228.

[20] B. J. Grummel, H. A. Mustain, Z. J. Shen, J. C. Elmes, and A. R. Hefner, "Reliability characterization of Au–In transient liquid phase bonding through electrical resistivity measurement," *IEEE Trans. Compon., Packag. Manuf. Technol.*, vol. 5, no. 12, pp. 1726–1733, Dec. 2015.

[21] N. S. Nobeen et al., "Transient liquid phase (TLP) bonding using Sn/Ag multilayers for high temperature applications," in *Proc. IEEE 15th Electron. Packag. Technol. Conf.*, 2013, pp. 647–652.

[22] K. S. Siow, "Are sintered silver joints ready for use as interconnect material in microelectronic packaging?," *J. Electron. Mater.*, vol. 43, no. 4, pp. 947–961, Apr. 2014.

[23] W. P. Lin, C.-H. Sha, and C. C. Lee, "40 μm flip-chip process using Ag–In transient liquid phase reaction," *IEEE Trans. Compon., Packag. Manuf. Technol.*, vol. 2, no. 6, pp. 903–908, Jun. 2012.

[24] S. W. Yoon, M. D. Glover, and K. Shiozaki, "Nickel-tin transient liquid phase bonding toward high-temperature operational power electronics in electrified vehicles," *IEEE Trans. Power Electron.*, vol. 28, no. 5, pp. 2448–2456, May 2013.

[25] K. Chu, Y. Sohn, and C. Moon, "A comparative study of Cn/Sn/Cu and Ni/Sn/Ni solder joints for low temperature stable transient liquid phase bonding," *Scripta Materialia*, vol. 109, pp. 113–117, Dec. 2015.

[26] T.-T. Luu, A. Duan, K. E. Aasmundtveit, and N. Hoivik, "Optimized Cu-Sn wafer-level bonding using intermetallic phase characterization," *J. Electron. Mater.*, vol. 42, no. 12, pp. 3582–3592, Dec. 2013.

[27] H. Chen, T. Hu, M. Li, and Z. Zhao, "Cu@Sn core–shell structure powder preform for high-temperature applications based on transient liquid phase bonding," *IEEE Trans. Power Electron.*, vol. 32, no. 1, pp. 441–451, Jan. 2017.

[28] H. Tatsumi, A. Lis, H. Yamaguchi, Y. Kashiba, and A. Hirose, "Evaluation of stiffness-reduced joints by transient liquid-phase sintering of copper-solder-resin composite for SiC die-attach applications," *IEEE Trans. Compon., Packag. Manuf. Technol.*, vol. 9, no. 10, pp. 2111–2121, Oct. 2019.

[29] J.-H. Park, J. Park, and K.-W. Paik, "Low temperature transient liquid phase (TLP) bonding using eutectic Sn-In solder anisotropic conductive films (ACFs) for flexible ultrasound transducer," in *Proc. IEEE 69th Electron. Compon. Technol. Conf.*, 2019, pp. 2213–2218.

[30] J. Cho, R. Sheikhi, S. Mallampati, L. Yin, and D. Shaddock, "Bismuth-based transient liquid phase (TLP) bonding as high-temperature lead-free solder alternatives," in *Proc. IEEE 67th Electron. Compon. Technol. Conf.*, 2017, pp. 1553–1559.

[31] P. Natzke, U. Grossner, J. Janczak-Rusch, and L. Jeurgens, "Thin layer Ag-Sn transient liquid phase bonding using magnetron sputtering for chip to baseplate bonding," in *Proc. IEEE 5th Workshop Wide Bandgap Power Devices Appl.*, 2017, pp. 165–170.

[32] F. Hou et al., "Microchannel thermal management system with two-phase flow for power electronics over 500 W/cm^2 heat dissipation," *IEEE Trans. Power Electron.*, vol. 35, no. 10, pp. 10592–10600, Oct. 2020.

[33] F. Hou et al., "Experimental evaluation of a compact two-phase cooling system for high heat flux electronic packages," *Appl. Thermal Eng.*, vol. 163, 2019, Art. no. 114338.

[34] M. Zhang et al., "Size-dependent melting point depression of nanostructures: Nanocalorimetric measurements," *Phys. Rev. B*, vol. 62, no. 15, pp. 10548–10557, Oct. 2000.

[35] Q. Jiang, S. H. Zhang, and J. C. Li, "Grain size-dependent diffusion activation energy in nanomaterials," *Solid State Commun.*, vol. 130, no. 9, pp. 581–584, Jun. 2004.

[36] K. Katayama, H. Nomura, H. Ogata, and T. Eitoku, "Diffusion coefficients for nanoparticles under flow and stop-flow conditions," *Phys. Chem. Chem. Phys.*, vol. 11, no. 44, pp. 10494–10499, 2009.

[37] S. Wang, H. Ji, M. Li, and C. Wang, "Fabrication of interconnects using pressureless low temperature sintered Ag nanoparticles," *Mater. Lett.*, vol. 85, pp. 61–63, Oct. 2012.

[38] H. Zhang et al., "Effects of sintering pressure on the densification and mechanical properties of nanosilver double-side sintered power module," *IEEE Trans. Compon., Packag. Manuf. Technol.*, vol. 9, no. 5, pp. 963–972, May 2019.

[39] J. G. Bai, Z. Z. Zhang, J. N. Calata, and G.-Q. Lu, "Low-temperature sintered nanoscale silver as a novel semiconductor device-metallized substrate interconnect material," *IEEE Trans. Compon. Packag. Technol.*, vol. 29, no. 3, pp. 589–593, Sep. 2006.

[40] J. G. Bai, J. Yin, Z. Zhang, G.-Q. Lu, and J. D. van Wyk, "High-temperature operation of SiC power devices by low-temperature sintered silver die-attachment," *IEEE Trans. Adv. Packag.*, vol. 30, no. 3, pp. 506–510, Aug. 2007.

[41] Z. Zhang, "Processing and characterization of micro-scale and nanoscale silver paste for power semiconductor device attachment," Ph.D. dissertation, Dept. of Elect. Comput. Eng., Virginia Tech., Blacksburg, VA, USA. Accessed: Sep. 2, 2015. [Online]. Available: https://vtechworks.lib.vt.edu/handle/10919/28902

[42] J. R. Groza, *Nanostructured Materials: Processing, Properties and Potential Applications*, C. C. Koch, Ed. Park Ridge, NJ, USA: Noyes Publication, 2002.

[43] J. Yeom, H. Zhang, C.-F. Li, and K. Suganuma, "Fast and low-temperature sintering of Ag paste due to nanoparticles formed in situ," *J. Mater. Sci., Mater. Electron.*, vol. 30, no. 19, pp. 18080–18087, Oct. 2019.

[44] W. Guo, Z. Zeng, X. Zhang, P. Peng, and S. Tang, "Low-temperature sintering bonding using silver nanoparticle paste for electronics packaging," *J. Nanomater.*, vol. 2015, Jan. 2015, Art. no. 10.

[45] Z. Z. Fang and H. Wang, "Densification and grain growth during sintering of nanosized particles," *Int. Mater. Rev.*, vol. 53, no. 6, pp. 326–352, Nov. 2008.

[46] J. Yan, "A review of sintering-bonding technology using ag nanoparticles for electronic packaging," *Nanomaterials*, vol. 11, no. 4, Apr. 2021, Art. no. 927.

[47] H. Zhang et al., "Microstructural and mechanical evolution of silver sintering die attach for SiC power devices during high temperature applications," *J. Alloys Compounds*, vol. 774, pp. 487–494, Feb. 2019.

[48] Y.-S. Lin et al., "Fine-pitch 30 μm Cu-Cu bonding using electroless nano-Ag," in *Proc. IEEE 73rd Electron. Compon. Technol. Conf.*, 2023, pp. 1115–1118.

[49] J. Zurcher et al., "All-copper flip chip interconnects by pressureless and low temperature nanoparticle sintering," in *Proc. IEEE 66th Electron. Compon. Technol. Conf.*, 2016, pp. 343–349.

[50] S. Magdassi, M. Grouchko, and A. Kamyshny, "Copper nanoparticles for printed electronics: Routes towards achieving oxidation stability," *Materials*, vol. 3, no. 9, pp. 4626–4638, Sep. 2010.

[51] B. Khodashenas and H. R. Ghorbani, "Synthesis of copper nanoparticles: An overview of the various methods," *Korean J. Chem. Eng.*, vol. 31, no. 7, pp. 1105–1109, Jul. 2014.

[52] M. A. Asoro, D. Kovar, and P. J. Ferreira, "Effect of surface carbon coating on sintering of silver nanoparticles: In situ TEM observations," *Chem. Commun.*, vol. 50, no. 37, pp. 4835–4838, Apr. 2014.

[53] N. G. Semaltianos, "Nanoparticles by laser ablation," *Crit. Rev. Solid State Mater. Sci.*, vol. 35, no. 2, pp. 105–124, May 2010.

[54] Z. Liu et al., "Cu-Cu bonding by Ag nanostructure at low temperature of 180°C," in *Proc. IEEE 17th Proc. IEEE Electron. Packag. Technol. Conf.*, 2015, pp. 1–4.

[55] Q. Jia et al., "Sintering mechanism of a supersaturated Ag–Cu nanoalloy film for power electronic packaging," *ACS Appl. Mater. Interfaces*, vol. 12, no. 14, pp. 16743–16752, Apr. 2020.

[56] Z. Zhang and G.-Q. Lu, "Pressure-assisted low-temperature sintering of silver paste as an alternative die-attach solution to solder reflow," *IEEE Trans. Electron. Packag. Manuf.*, vol. 25, no. 4, pp. 279–283, Oct. 2002.

[57] W. Schmitt, L. M. Chew, and R. Miller, "Pressure-less sintering on large dies using infrared radiation and optimized silver sinter paste," in *Proc. IEEE 68th Electron. Compon. Technol. Conf.*, 2018, pp. 539–544.

[58] K. S. Siow, "Mechanical properties of nano-silver joints as die attach materials," *J. Alloys Compounds*, vol. 514, pp. 6–19, Feb. 2012.

[59] M. Tobita, Y. Yasuda, E. Ide, J. Ushio, and T. Morita, "Optimal design of coating material for nanoparticles and its application for low-temperature interconnection," *J. Nanoparticle Res.*, vol. 12, no. 6, pp. 2135–2144, Aug. 2010.

[60] J. Liu, W. Lv, Y. Mou, C. Chen, and Y. Kang, "Coalescence behavior of Cu nanoparticles during sintering: Based on atomic scale to macro scale," *J. Mater. Res. Technol.*, vol. 27, pp. 2490–2507, Nov. 2023.

[61] D. Hu, Z. Cui, J. Fan, X. Fan, and G. Zhang, "Thermal kinetic and mechanical behaviors of pressure-assisted Cu nanoparticles sintering: A molecular dynamics study," *Results Phys.*, vol. 19, Dec. 2020, Art. no. 103486.

[62] D. Hu et al., "High temperature viscoplastic deformation behavior of sintered nanocopper paste used in power electronics packaging: Insights from constitutive and multi-scale modelling," *J. Mater. Res. Technol.*, vol. 26, pp. 3183–3200, Sep. 2023.

[63] H. Tatsumi, C. R. Kao, and H. Nishikawa, "Solid-state bonding behavior between surface-nanostructured Cu and Au: A molecular dynamics simulation," *Sci. Rep.*, vol. 12, no. 1, Jul. 2022, Art. no. 12755.

[64] B. Cheng and A. H. W. Ngan, "The sintering and densification behaviour of many copper nanoparticles: A molecular dynamics study," *Comput. Mater. Sci.*, vol. 74, pp. 1–11, Jun. 2013.

[65] S.-J. L Kang, *Sintering: Densification, Grain Growth and Microstructure*. Amsterdam, The Netherlands: Elsevier, 2004.

[66] E. Ide, S. Angata, A. Hirose, and K. F. Kobayashi, "Metal–metal bonding process using Ag metallo-organic nanoparticles," *Acta Materialia*, vol. 53, no. 8, pp. 2385–2393, May 2005.

[67] T. Morita, E. Ide, Y. Yasuda, A. Hirose, and K. Kobayashi, "Study of bonding technology using silver nanoparticles," *Jpn. J. Appl. Phys.*, vol. 47, no. 8R, Aug. 2008, Art. no. 6615.

[68] T. G. Lei, J. N. Calata, G.-Q. Lu, X. Chen, and S. Luo, "Low-temperature sintering of nanoscale silver paste for attaching large-area (>100 mm^2) chips," *IEEE Trans. Compon. Packag. Technol.*, vol. 33, no. 1, pp. 98–104, Mar. 2010.

[69] J. Yan et al., "Pressureless bonding process using Ag nanoparticle paste for flexible electronics packaging," *Scripta Materialia*, vol. 66, no. 8, pp. 582–585, Apr. 2012.

[70] M. Knoerr and A. Schletz, "Power semiconductor joining through sintering of silver nanoparticles: Evaluation of influence of parameters time, temperature and pressure on density, strength and reliability," in *Proc. 6th Int. Conf. Integr. Power Electron. Syst.*, 2010, pp. 1–6.

[71] M. Li, Y. Xiao, Z. Zhang, and J. Yu, "Bimodal sintered silver nanoparticle paste with ultrahigh thermal conductivity and shear strength for high temperature thermal interface material applications," *ACS Appl. Mater. Interfaces*, vol. 7, no. 17, pp. 9157–9168, May 2015.

[72] S. Sakamoto, S. Nagao, and K. Suganuma, "Thermal fatigue of Ag flake sintering die-attachment for Si/SiC power devices," *J. Mater. Sci., Mater. Electron.*, vol. 24, no. 7, pp. 2593–2601, Jul. 2013.

[73] H. Zheng, D. Berry, K. D. T. Ngo, and G.-Q. Lu, "Chip-bonding on copper by pressureless sintering of nanosilver paste under controlled atmosphere," *IEEE Trans. Compon., Packag. Manuf. Technol.*, vol. 4, no. 3, pp. 377–384, Mar. 2014.

[74] F. Ternero, L. G. Rosa, P. Urban, J. M. Montes, and F. G. Cuevas, "Influence of the total porosity on the properties of sintered materials—A review," *Metals*, vol. 11, no. 5, Apr. 2021, Art. no. 730.

[75] S. A. Paknejad and S. H. Mannan, "Review of silver nanoparticle based die attach materials for high power/temperature applications," *Microelectron. Rel.*, vol. 70, pp. 1–11, Mar. 2017.

[76] J. Yeom et al., "Ag particles for sinter bonding: Flakes or spheres?," *Appl. Phys. Lett.*, vol. 114, no. 25, Jun. 2019, Art. no. 253103.

[77] W. Li et al., "Pressureless sinter-joining of micron-Ag flake pastes at 160°C enabled by solvent and interface engineering," *J. Mater. Process. Technol.*, vol. 322, Dec. 2023, Art. no. 118207.

[78] C. Wang et al., "Low temperature sintered silver nanoflake paste for power device packaging and its anisotropic sintering mechanism," *ACS Appl. Electron. Mater.*, vol. 3, no. 12, pp. 5365–5373, Dec. 2021.

[79] S. Li et al., "Sintering mechanism of Ag nanoparticle-nanoflake: A molecular dynamics simulation," *J. Mater. Res. Technol.*, vol. 16, pp. 640–655, Jan. 2022.

[80] R. Luo et al., "Molecular dynamics simulations on mechanical behaviors of sintered nanocopper in power electronics packaging," *Microelectron. Rel.*, vol. 152, Jan. 2024, Art. no. 115284.

[81] L. D. Marks and L. Peng, "Nanoparticle shape, thermodynamics and kinetics," *J. Phys., Condens. Matter*, vol. 28, no. 5, Feb. 2016, Art. no. 053001.

[82] R. Riva, C. Buttay, B. Allard, and P. Bevilacqua, "Migration issues in sintered-silver die attaches operating at high temperature," *Microelectron. Rel.*, vol. 53, no. 9/11, pp. 1592–1596, Sep. 2013.

[83] Z. Jin, F. Huo, J. Wang, X. Liu, Y. C. Chan, and H. Nishikawa, "Electromigration-induced microstructure evolution and failure mechanism of sintered nano-Ag joint," *Mater. Characterization*, vol. 205, Nov. 2023, Art. no. 113309.

[84] J. Li, Q. Liang, C. Chen, T. Shi, G. Liao, and Z. Tang, "Cu-Cu bonding by low-temperature sintering of self-healable Cu nanoparticles," in *Proc. IEEE 69th Electron. Compon. Technol. Conf.*, 2019, pp. 661–666.

[85] J. Liu, H. Chen, H. Ji, and M. Li, "Highly conductive Cu–Cu joint formation by low-temperature sintering of formic acid-treated Cu nanoparticles," *ACS Appl. Mater. Interfaces*, vol. 8, no. 48, pp. 33289–33298, Dec. 2016.

[86] Y. Kamikoriyama, H. Imamura, A. Muramatsu, and K. Kanie, "Ambient aqueous-phase synthesis of copper nanoparticles and nanopastes with low-temperature sintering and ultra-high bonding abilities," *Sci. Rep.*, vol. 9, no. 1, Jan. 2019, Art. no. 899.

[87] Y. Gao et al., "Novel copper particle paste with self-reduction and self-protection characteristics for die attachment of power semiconductor under a nitrogen atmosphere," *Mater. Des.*, vol. 160, pp. 1265–1272, Dec. 2018.

[88] J. Li et al., "Low-temperature and low-pressure Cu–Cu bonding by highly sinterable Cu nanoparticle paste," *Nanoscale Res. Lett.*, vol. 12, no. 1, Dec. 2017, Art. no. 255.

[89] Y. Jianfeng, Z. Guisheng, H. Anming, and Y. N. Zhou, "Preparation of PVP coated Cu NPs and the application for low-temperature bonding," *J. Mater. Chem.*, vol. 21, no. 40, 2011, Art. no. 15981.

[90] B. Zhang, "Low temperature sintering of Cu nanoparticle—Mechanism and die attach application," Ph.D. dissertation, Microelectron. Dept., Delft Univ. of Technol., Delft, The Netherlands, 2020.

[91] Y. Zuo, S. Carter-Searjeant, M. Green, L. Mills, and S. H. Mannan, "High bond strength Cu joints fabricated by rapid and pressureless in situ reduction-sintering of Cu nanoparticles," *Mater. Lett.*, vol. 276, Oct. 2020, Art. no. 128260.

[92] H. Nakako, D. Ishikawa, C. Sugama, Y. Kawana, M. Negishi, and Y. Ejiri, "Sintering copper die-bonding paste curable under pressureless conditions," in *Proc. Int. Exhib. Conf. Power Electron., Intell. Motion, Renewable Energy Energy Manage.*, 2017, pp. 1–5.

[93] T. Yamakawa, T. Takemoto, M. Shimoda, H. Nishikawa, K. Shiokawa, and N. Terada, "Influence of joining conditions on bonding strength of joints: Efficacy of low-temperature bonding using Cu nanoparticle paste," *J. Electron. Mater.*, vol. 42, no. 6, pp. 1260–1267, Jun. 2013.

[94] L. Del Carro, J. Zurcher, U. Drechsler, I. E. Clark, G. Ramos, and T. Brunschwiler, "Low-temperature dip-based all-copper interconnects formed by pressure-assisted sintering of copper nanoparticles," *IEEE Trans. Compon., Packag. Manuf. Technol.*, vol. 9, no. 8, pp. 1613–1622, Aug. 2019.

[95] Y. Tian et al., "Sintering mechanism of the Cu–Ag core–shell nanoparticle pastes at low temperature in ambient air," *RSC Adv.*, vol. 6, no. 94, pp. 91783–91790, 2016.

[96] H. Ji, J. Zhou, M. Liang, H. Lu, and M. Li, "Ultra-low temperature sintering of Cu@Ag core-shell nanoparticle paste by ultrasonic in air for high-temperature power device packaging," *Ultrasonics Sonochem.*, vol. 41, pp. 375–381, Mar. 2018.

[97] H. Yan, P. Liang, Y. Mei, and Z. Feng, "Brief review of silver sinter-bonding processing for packaging high-temperature power devices," *Chin. J. Elect. Eng.*, vol. 6, no. 3, pp. 25–34, Sep. 2020.

[98] Y. Mei, Y. Cao, G. Chen, X. Li, G.-Q. Lu, and X. Chen, "Rapid sintering nanosilver joint by pulse current for power electronics packaging," *IEEE Trans. Device Mater. Rel.*, vol. 13, no. 1, pp. 258–265, Mar. 2013.

[99] Y.-H. Mei, Y. Cao, G. Chen, X. Li, G.-Q. Lu, and X. Chen, "Characterization and reliability of sintered nanosilver joints by a rapid current-assisted method for power electronics packaging," *IEEE Trans. Device Mater. Rel.*, vol. 14, no. 1, pp. 262–267, Mar. 2014.

[100] G.-Q. Lu, W. Li, Y. Mei, G. Chen, X. Li, and X. Chen, "Characterizations of nanosilver joints by rapid sintering at low temperature for power electronic packaging," *IEEE Trans. Device Mater. Rel.*, vol. 14, no. 2, pp. 623–629, Jun. 2014.

[101] G. D. Liu, C. Wang, and J. Swingler, "Laser-assisted sintering of silver nanoparticle paste for bonding of silicon to DBC for high-temperature electronics packaging," *IEEE Trans. Compon., Packag. Manuf. Technol.*, vol. 11, no. 3, pp. 522–529, Mar. 2021.

[102] W. Liu, C. Wang, C. Wang, X. Jiang, and X. Huang, "Laser sintering of nano-Ag particle paste for high-temperature electronics assembly," *IEEE Trans. Compon., Packag. Manuf. Technol.*, vol. 7, no. 7, pp. 1050–1057, Jul. 2017.

[103] B. Zhang et al., "In-air sintering of copper nanoparticle paste with pressure-assistance for die attachment in high power electronics," *J. Mater. Sci., Mater. Electron.*, vol. 32, no. 4, pp. 4544–4555, Feb. 2021.

[104] X. Liu et al., "Microstructural evolution, fracture behavior and bonding mechanisms study of copper sintering on bare DBC substrate for SiC power electronics packaging," *J. Mater. Res. Technol.*, vol. 19, pp. 1407–1421, Jul. 2022.

[105] T. Furukawa et al., "High power density side-gate HiGT modules with sintered Cu having superior high-temperature reliability to sintered Ag," in *Proc. 29th Int. Symp. Power Semicond. Devices IC's*, 2017, pp. 263–266.

[106] Y. Kobayashi, T. Shirochi, T. Maeda, Y. Yasuda, and T. Morita, "Microstructure of metallic copper nanoparticles/metallic disc interface in metal–metal bonding using them," *Surf. Interface Anal.*, vol. 45, no. 9, pp. 1424–1428, Sep. 2013.

[107] T. Ishizaki, K. Akedo, T. Satoh, and R. Watanabe, "Pressure-free bonding of metallic plates with Ni affinity layers using Cu nanoparticles," *J. Electron. Mater.*, vol. 43, no. 3, pp. 774–779, Mar. 2014.

[108] T. Morita and Y. Yasuda, "New bonding technique using copper oxide materials," *Mater. Trans.*, vol. 56, no. 6, pp. 878–882, 2015.

[109] D. Ishikawa et al., "Copper die-bonding sinter paste: Sintering and bonding properties," in *Proc. 7th Electron. Syst.-Integr. Technol. Conf.*, 2018, pp. 1–10.

[110] D. Ishikawa et al., "Bonding strength of Cu sinter die-bonding paste ON Ni, Cu, Ag, and Au surfaces under pressureless bonding process," *Trans. Jpn. Inst. Electron. Packag.*, vol. 13, pp. E19–017–1–E19–017–11, 2020.

[111] R. Gao, S. He, Y.-A. Shen, and H. Nishikawa, "Effect of substrates on fracture mechanism and process optimization of oxidation–reduction bonding with copper microparticles," *J. Electron. Mater.*, vol. 48, no. 4, pp. 2263–2271, Apr. 2019.

[112] C. Herold, M. Schaefer, F. Sauerland, T. Poller, J. Lutz, and O. Schilling, "Power cycling capability of modules with SiC-diodes," in *Proc. 8th Int. Conf. Integr. Power Electron. Syst.*, 2014, pp. 1–6.

[113] Y. Gao, C. Chen, S. Nagao, K. Suganuma, A. S. Bahman, and F. Iannuzzo, "Highly reliable package using Cu particles sinter paste for next generation power devices," in *Proc. Int. Exhib. Conf. Power Electron., Intell. Motion, Renewable Energy Energy Manage.*, 2019, pp. 1–4.

[114] Y. Gao et al., "Reliability analysis of sintered Cu joints for SiC power devices under thermal shock condition," *Microelectron. Rel.*, vol. 100–101, Sep. 2019, Art. no. 113456.

[115] K. Yasui et al., "Improvement of power cycling reliability of 3.3 kV full-SiC power modules with sintered copper technology for T_j, max = 175°C," in *Proc. IEEE 30th Int. Symp. Power Semicond. Devices ICs*, 2018, pp. 455–458.

[116] C. Chen et al., "Development of micron-sized Cu–Ag composite paste for oxidation-free bare Cu bonding in air condition and its deterioration mechanism during aging and power cycling tests," *J. Mater. Res. Technol.*, vol. 24, pp. 8967–8983, May 2023.

[117] T. Ishizaki et al., "Reliability of Cu nanoparticle joint for high temperature power electronics," *Microelectron. Rel.*, vol. 54, no. 9/10, pp. 1867–1871, Sep. 2014.

[118] J. Xin et al., "High performance Cu sintering joint for power devices enabled by in-situ generation of Cu particles with multi-level hierarchical structures," *J. Mater. Process. Technol.*, vol. 329, Aug. 2024, Art. no. 118435.